

On the anti-aliasing properties of entropy filtering for under-resolved turbulent flows

T. Dzanic^{a,*}, W. Trojak^{b,c} and F. D. Witherden^a


^a*Department of Ocean Engineering, Texas A&M University, College Station, TX 77843*

^b*Department of Aeronautics, Imperial College London, South Kensington, London, SW7 2AZ*

^c*IBM Research, The Hartree Centre, Daresbury, WA4 4AD*

arXiv:2302.13359v1 [math.NA] 26 Feb 2023

*Corresponding author

 tdzanic@tamu.edu (T. Dzanic)

ORCID(s): 0000-0003-3791-1134 (T. Dzanic); 0000-0002-4407-8956 (W. Trojak); 0000-0003-2343-412X (F.D. Witherden)

1. Introduction

Discontinuous spectral element methods (DSEM) offer an attractive approach for simulating turbulent flow phenomena due to their geometric flexibility, arbitrarily high-order accuracy, and computational efficiency. However, for increasingly large Reynolds number flows, the computational cost of resolving all of the statistically significant physical scales becomes prohibitively large, such that it is necessary in many cases to perform simulations that are under-resolved with respect to the underlying flow physics. For nodal DSEM approximations of these under-resolved flows, the collocation projection of the nonlinear flux onto the space spanned by the solution approximation can introduce aliasing errors which can result in numerical instabilities, leading to nonphysical solutions or the failure of the scheme altogether. These errors are typically mitigated through the addition of some anti-aliasing or numerical stabilization techniques such as Galerkin projection, filtering, the use of a spectral vanishing viscosity, or through switching to a split skew-symmetric formulation (see Cox et al. [1] and the references therein). These methods vary in their performance and robustness, often coming with either a notable increase in the computational cost or free parameters which may require extensive tuning.

In Dzanic and Witherden [2], an entropy-based adaptive filtering approach was introduced for the purpose of mitigating numerical instabilities stemming from high-order approximations of discontinuous flow features (i.e., shocks). It was observed by the authors that this parameter-free shock-capturing approach, referred to as entropy filtering, also allowed for the robust simulation of high Reynolds number flows on under-resolved meshes that would typically be unstable due to aliasing errors. We posit that this is a result of aliasing errors manifesting as violations of a local minimum entropy principle, which is supported by the observations of Honein and Moin [3], such that entropy filtering may adequately perform as an anti-aliasing technique separately from its purpose as a shock-capturing approach. This technical note explores this effect and presents a comparison to standard anti-aliasing approaches through implicit large eddy simulations of a NACA0021 in deep stall from the DESider project [4] as presented by Park et al. [5], a case notorious for aliasing driven instabilities in high-order methods that requires a substantial amount of numerical stabilization for the given setup.

2. Methodology

2.1. Discretization

The compressible Navier–Stokes equations were discretized using the flux reconstruction scheme of Huynh [6] utilizing the equivalent discontinuous Galerkin [7] correction functions. The order of the scheme, denoted by \mathbb{P}_p for some order p , is taken as the maximal order of the solution basis. Third-order (\mathbb{P}_3) and fourth-order (\mathbb{P}_4) approximations were considered in this work, corresponding to nominally fourth-order and fifth-order accurate spatial discretizations, respectively. Temporal integration was performed using a fourth-order, four stage Runge-Kutta scheme.

2.2. Anti-aliasing techniques

The entropy filtering approach was compared to two standard anti-aliasing techniques: Galerkin projection and modal filtering. For the Galerkin projection approach (sometimes referred to as over-integration), the goal for some nonlinear flux function $\mathbf{F}(\mathbf{u})$ of the solution \mathbf{u} is to find the flux polynomial $\hat{\mathbf{f}}(\mathbf{x})$ that minimizes the norm $\|\mathbf{F}(\mathbf{u}(\mathbf{x})) - \hat{\mathbf{f}}(\mathbf{x})\|_2$, i.e., the L^2 projection of $\mathbf{F}(\mathbf{u})$ onto the \mathbb{P}_{p+1} polynomial space spanned by $\hat{\mathbf{f}}(\mathbf{x})$ [8]. For non-polynomial flux functions, this projection usually cannot be performed exactly, but it may be approximated utilizing a suitably-strong quadrature rule. Typically, the more under-resolved the flow is, the stronger the quadrature rule has to be to mitigate aliasing errors, such that for highly under-resolved flows, the cost of computing this projection may become substantial. In this work, we utilize Gaussian quadrature rules to compute the projection with the notation GP- \mathbb{Q}_q referring to Galerkin projection with a q -th degree quadrature rule. For a more in-depth description of this approach, the reader is referred to Park et al. [5], Section II.D. \mathbb{Q}_9 and \mathbb{Q}_{11} GP was used for the \mathbb{P}_3 and \mathbb{P}_4 approximations, respectively, as this was deemed to be the necessary amount of anti-aliasing to stabilize the solution over the simulation time [5].

For the modal filtering approach, denoted by MF, the goal is to mitigate aliasing driven instabilities by explicitly filtering the high-frequency content from the solution as these errors tend to manifest at higher frequencies [1]. In this approach, the solution is transformed to its modal form and a filtering operation $H(\mathbf{u})$ is applied, such that the filtered solution $\tilde{\mathbf{u}}(\mathbf{x})$ can be given as

$$\tilde{\mathbf{u}}(\mathbf{x}) = \sum_{i=1}^{N_s} H(\hat{\mathbf{u}}_i) \phi_i(\mathbf{x}), \quad (1)$$

where $\phi_i(\mathbf{x})$ are a set of N_s orthogonal polynomials (typically with respect to the unit measure) and $\hat{\mathbf{u}}_i$ are their associated modal coefficients. A standard choice of filter kernel is the exponential filter [7], given as

$$H_i(\hat{\mathbf{u}}_i) = \begin{cases} \hat{\mathbf{u}}_i, & \text{if } \eta_i \leq \eta_c, \\ \hat{\mathbf{u}}_i \exp \left[-\kappa \left(\frac{\eta_i - \eta_c}{\eta_m - \eta_c} \right)^s \right], & \text{else,} \end{cases} \quad (2)$$

where $\kappa \approx \log \epsilon$ for some value of machine precision ϵ , s is some even integer representing the filter order, η_i is the maximal order of the i -th basis function, η_c is the cutoff order, and $\eta_m = p + 1$ is the maximal order. The parameters were chosen as $\kappa = 32$, $\eta_c = 0$, and $s = 8$ (for \mathbb{P}_3) and $s = 6$ (for \mathbb{P}_4), with the filter applied every $N = 20$ time steps. These values were found by systematically modulating each component to find a set of values that stabilized the solution over the simulation period. We remark here that it is unlikely that these are the optimal parameters for this approach, and there could be values of these parameters that yield a stable approach with more accurate results. However, this is the typical drawback of stabilization techniques that have free parameters—it can be extremely costly to attempt to optimize these parameters over many simulations, and, without a proper point of reference, it is ambiguous as to which parameters result in more accurate predictions.

These two anti-aliasing approaches were compared to the entropy filter, denoted by EF. In this approach, the filtering kernel is computed adaptively based on the solution's ability to preserve certain invariants of the system such as the positivity of density and pressure and a local discrete minimum entropy principle [2]. This adaptive method, which does not require any problem-dependent tunable parameters, was implemented in the context of a second-order exponential filter applied at each stage of the temporal scheme, given as

$$H_i(\hat{\mathbf{u}}_i) = \hat{\mathbf{u}}_i \exp(-\zeta \eta_i^2), \quad (3)$$

where ζ is the filter strength. This filter strength is computed via an element-wise nonlinear optimization problem that finds the minimum necessary filter strength such that the discrete nodal solution values have positive density ($\rho > 0$), positive pressure ($P > 0$), and an entropy greater than some minimum threshold ($\sigma > \sigma_{\min}$). For an in-depth overview of this approach, the reader is referred to Dzanic and Witherden [2], Section 3. We note that along with some improvements for the nonlinear optimization process [9], the current implementation of this approach slightly differs from the original work in that the specific physical entropy is used ($\sigma = P\rho^{-\gamma}$, where γ is the ratio of specific heats), no operator splitting is performed for the Navier–Stokes equations, and the temporal integration methods are not restricted to strong stability preserving schemes.

2.3. Problem setup

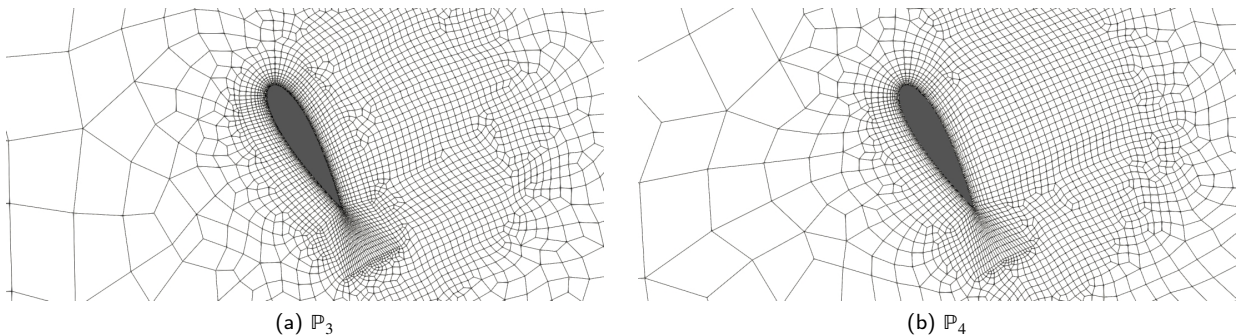


Figure 1: Cross-section of the mesh used for the \mathbb{P}_3 (left) and \mathbb{P}_4 (right) simulations.

The problem setup consists of a NACA0021 airfoil operating at a Reynolds number of $Re = 270,000$, Mach number of $M = 0.1$, and an angle of attack $\alpha = 60^\circ$. The unstructured hexahedral meshes of Park et al. [5] were used, shown in Fig. 1, consisting of a finer \mathbb{P}_3 mesh (323,360 hexahedral elements) and a coarser \mathbb{P}_4 mesh (206,528 hexahedral elements) with an aspect ratio of 4. The \mathbb{P}_4 mesh was appropriately coarsened such that the degrees of freedom and the relative nodal spacing between the two approximation orders were roughly equal, and both meshes were generated such that the wall-normal spacing of the first solution point was $y^+ \approx 1$. The simulation was initialized with \mathbb{P}_1 at $Re = 27,000$ and run until a characteristic time of $t_c = c/U_\infty = 50$, where c is the chord and U_∞ is the freestream velocity, with double precision arithmetic. The Reynolds number and approximation order were then

increased to the operating conditions and the anti-aliasing methods of choice were applied. Without any anti-aliasing approach, the simulation quickly diverged. The flow was allowed to develop until $t_c = 100$, and then averaging was performed over the range $t_c \in [100, 300]$. Increasing the averaging period was found to have a minimal effect on the results.

Due to the different stabilizing effects of the various anti-aliasing approaches, different maximum time steps were permissible. For the GP approach, the maximum allowable time step was $\Delta t = 2 \cdot 10^{-5}$, whereas the MF approach only allowed a time step of $\Delta t = 1 \cdot 10^{-5}$. However, due to its additional nonlinear stability properties, the EF approach allowed a larger time step of $\Delta t = 5 \cdot 10^{-5}$. These factors contribute to the overall cost of the simulations in addition to the per-time-step cost of the anti-aliasing approach.

3. Results

The efficacy of the anti-aliasing techniques was evaluated with respect to its ability to predict the average surface pressure coefficient distribution and the power spectral density (PSD) of the lift coefficient in comparison to the experimental results of Swalwell [10]. The PSD was computed using Welch's averaged periodogram method with a sampling rate of $0.00625t_c$, window length of 4096, and a shift of 10, and the comparison was performed with respect to the ability to predict the frequencies of the primary and secondary peaks in the PSD.

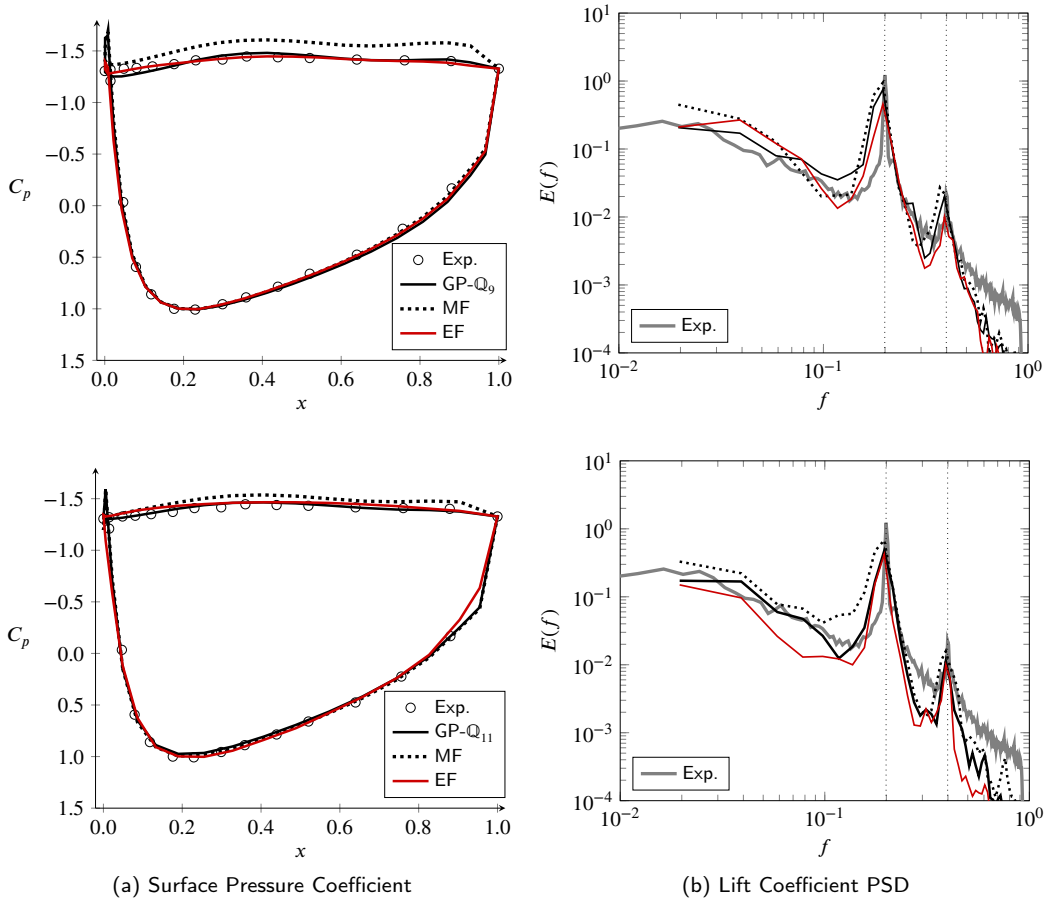


Figure 2: Average surface pressure coefficient distribution (left column) and lift coefficient power spectral density (right column) computed using a \mathbb{P}_3 approximation (top row) and \mathbb{P}_4 approximation (bottom row) with Galerkin projection (GP), modal filtering (MF), and entropy filtering (EF). Experimental results of Swalwell [10] shown for reference. Primary and secondary PSD peaks in the experimental data shown as vertical dotted lines.

The average surface pressure coefficient distribution and the PSD for the \mathbb{P}_3 experiments are shown in the top row of Fig. 2. Both the GP and EF approaches yielded good predictions of the surface pressure coefficient distribution as well as the frequencies of the primary and secondary peaks in the PSD. However, the MF approach was not as performant,

yielding poor predictions of the surface pressure coefficient on the suction side of the airfoil and marginally worse predictions of the frequency of the secondary peak in the PSD.

The results of the \mathbb{P}_4 experiments are similarly shown in the bottom row of Fig. 2. Much like with the \mathbb{P}_3 experiments, both the GP and EF approaches yielded good predictions in terms of the surface pressure coefficient distribution and the peaks in the PSD. In comparison to the \mathbb{P}_3 experiments, the MF approach performed notably better, with just marginally worse predictions of the surface pressure coefficient on the suction side of the airfoil than the other two approaches. Overall, all approaches yielded reasonable predictions in comparison to the experimental data.

A comparison of the computational cost of the various approaches is shown in Fig. 3 in terms of both the wall-clock time required to compute one time step and 10 flows over chord, respectively, on 16 NVIDIA V100 GPUs. Due to the large bandwidth and compute requirements of evaluating the projection, the cost of the GP approach was the highest both in terms of per time step and overall, requiring 288.5 GPU hours for \mathbb{P}_3 and 320 GPU hours for \mathbb{P}_4 . Furthermore, while the MF approach itself was the least costly per time step, the overall cost of the approach was still notably high due to the time step constraints imposed by the method, requiring 177.3 GPU hours for \mathbb{P}_3 and 240.1 GPU hours for \mathbb{P}_4 . In comparison, the EF approach was the most efficient overall, requiring 90.4 GPU hours for \mathbb{P}_3 and 121.6 GPU hours for \mathbb{P}_4 , primarily driven by the larger time steps afforded by the method.

In conclusion, the EF approach may offer an effective method for mitigating aliasing-driven instabilities in the simulation of under-resolved turbulent flows, yielding similar accuracy to the GP approach at a notably lower computational cost than both the GP and MF approaches. Furthermore, the increased stability afforded by the EF approach as well as the lack of tunable parameters allows for the robust and accurate simulation of these flows.

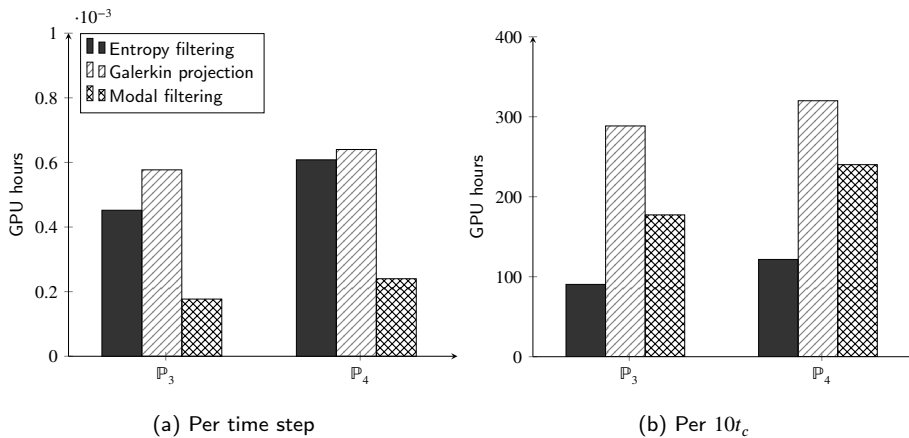


Figure 3: Wall clock time in NVIDIA V100 GPU hours per time step (left) and per 10 flows over chord (right) using a \mathbb{P}_3 and \mathbb{P}_4 approximation with varying anti-aliasing methods. Simulations performed on 16 NVIDIA V100 GPUs.

References

- [1] C. Cox, W. Trojak, T. Dzanic, F.D. Witherden, and A. Jameson. Accuracy, stability, and performance comparison between the spectral difference and flux reconstruction schemes. *Computers & Fluids*, 221:104922, May 2021. doi: 10.1016/j.compfluid.2021.104922.
- [2] Tarik Dzanic and Freddie D. Witherden. Positivity-preserving entropy-based adaptive filtering for discontinuous spectral element methods. *Journal of Computational Physics*, 468:111501, November 2022. doi: 10.1016/j.jcp.2022.111501.
- [3] Albert E. Honein and Parviz Moin. Higher entropy conservation and numerical stability of compressible turbulence simulations. *Journal of Computational Physics*, 201(2):531–545, December 2004. doi: 10.1016/j.jcp.2004.06.006.
- [4] Werner Haase, Marianna Braza, and Alistair Revell. *DESider – A European Effort on Hybrid RANS-LES Modelling*. Springer Berlin Heidelberg, 2009. doi: 10.1007/978-3-540-92773-0.
- [5] J. S. Park, F. D. Witherden, and P. E. Vincent. High-order implicit large-eddy simulations of flow over a NACA0021 aerofoil. *AIAA Journal*, 55(7):2186–2197, July 2017. doi: 10.2514/1.j055304.
- [6] H. T. Huynh. A flux reconstruction approach to high-order schemes including discontinuous Galerkin methods. In *18th AIAA Computational Fluid Dynamics Conference*. American Institute of Aeronautics and Astronautics, June 2007. doi: 10.2514/6.2007-4079.
- [7] Jan S. Hesthaven and Tim Warburton. *Nodal Discontinuous Galerkin Methods*. Springer New York, 2008. doi: 10.1007/978-0-387-72067-8.
- [8] A. Jameson, P. E. Vincent, and P. Castonguay. On the non-linear stability of flux reconstruction schemes. *Journal of Scientific Computing*, 50(2):434–445, April 2011. doi: 10.1007/s10915-011-9490-6.
- [9] Tarik Dzanic and Freddie D. Witherden. Positivity-preserving entropy filtering for the ideal magnetohydrodynamics equations. art. arXiv:2301.03129, January 2023.
- [10] Kartina Elise Swalwell. The effect of turbulence on stall of horizontal axis wind turbines. Master’s thesis, Monash University, 2005.